Cell Reports
Physical Science

CellPress
OPEN ACCESS

Article

A genipin crosslinked silk fibroin monolith by compression molding with recovering mechanical properties in physiological conditions

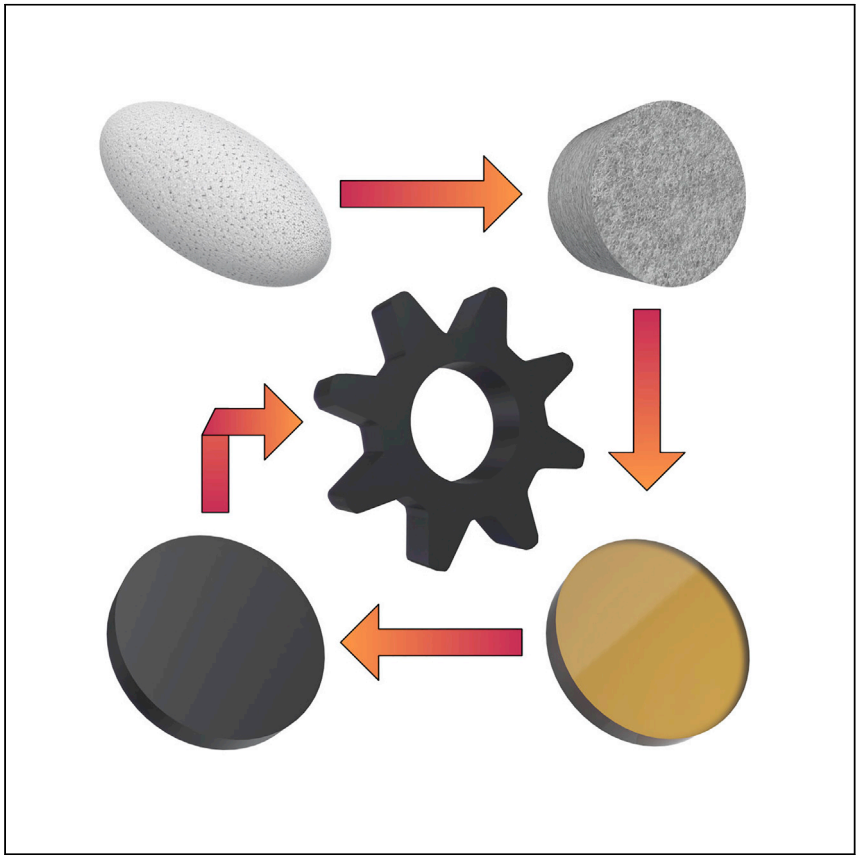

Silk monoliths have been previously reported as materials with impressive mechanical strength in dry environments, which greatly decreases in wet conditions. In this study, Bucciarelli et al. report a methodology based on the addition of genipin to a silk solution before the fabrication of the monolith and its successive exposure to water to trigger a crosslinking reaction. This allows silk monoliths to retain their mechanical properties in physiological conditions, extending the scope of their potential applications to structural ones.

Alessio Bucciarelli, Valentino Janigro, Yuejiao Yang, Giulia Fredi, Alessandro Pegoretti, Antonella Motta, Devid Maniglio

alessio.bucciarelli@nanotec.cnr.it

Highlights

Genipin is dispersed in solid fibroin monoliths

The water-triggered crosslinking improves the mechanical properties

The crosslinked material retains its shape up to 30 days in an enzymatic solution

Laser cutting helps the production of complex functional objects

Bucciarelli et al., Cell Reports Physical Science 2, 100605
October 20, 2021
https://doi.org/10.1016/j.xcrp.2021.100605

Cell Reports
Physical Science

CellPress
OPEN ACCESS

Article

A genipin crosslinked silk fibroin monolith by compression molding with recovering mechanical properties in physiological conditions

Alessio Bucciarelli,[1,4,*] Valentino Janigro,[2] Yuejiao Yang,[2] Giulia Fredi,[3] Alessandro Pegoretti,[3] Antonella Motta,[2] and Devid Maniglio[2]

SUMMARY

Fibroin monoliths, produced by compression molding starting from the protein powder, are known to achieve an impressive mechanical strength when tested in dry conditions. However, in the presence of water, the loss of structural integrity and mechanical performances is striking. Considering the bone scaffold applications for which this material is intended, this remarkable weakening after implantation strongly limits its usage to non-structural purposes. Here, we propose an approach that allows the recovery of mechanical properties and the retention of the shape in physiological conditions, due to a progressive chemical crosslinking triggered by genipin and humidity. Crosslinking does not hinder cell adhesion and proliferation, as suggested by a preliminary biological test, nor does it limit the machinability of the material, as demonstrated by producing complex-shaped objects through laser cutting. Overall, genipin-crosslinked solid fibroin is a reliable material that may be suitable for structural applications in physiological conditions.

INTRODUCTION

Silk is a fiber produced by several arthropods and used for the production of textiles since ancient times. Besides the traditional uses of silk, the isolation of the internal structural protein of the fiber, namely silk fibroin (SF), had led to the development of several materials with a core application in tissue engineering.[1–4] In fact, the combination of a unique set of properties such as a tunable mechanical strength, an excellent biocompatibility,[4–6] the optical transparency,[7–11] and the facile processability[12] makes the regenerated SF an optimal candidate for several bio-related applications. The structure of SF is semicrystalline, composed of β sheet crystallites with an ordered repetition of amino acids (heavy-chain domain, 300 kDa) and in an amorphous phase consisting of a less-ordered amino acid sequence (light-chain domain, 26 kDa).[6] The possibility to unfold the β sheets by denaturation and control the protein refolding allows us to tune the overall crystallinity and consequently the material properties.[6] This versatility in tissue engineering has been widely adopted to produce architectures with properties able to mimic the natural tissues.[13–15] For applications in bone tissue engineering, SF is commonly reinforced with fibers[14,16,17] or hydroxyapatite/bone powder.[15,16,18] However, among the different structures producible from silk, solid silk obtained by the application of high pressure and high temperature to mold the SF powder has been reported to possess an impressive mechanical strength (compressive modulus on the order of 1–2 GPa).[19–23]

[1]CNR-Nanotec, Institute of Nanotechnology, National Council of Research, via Monteroni, 73100 Lecce, Italy

[2]BIOtech Research Centre and European Institute of Excellence on Tissue Engineering and Regenerative Medicine, Department of Industrial Engineering, University of Trento, Via delle Regole 101, 38123 Trento, Italy

[3]Polymers and Composites Laboratory, Department of Industrial Engineering and INSTM Research Unit, University of Trento, Via Sommarive 9, 38123 Trento, Italy

[4]Lead contact

*Correspondence: alessio.bucciarelli@nanotec.cnr.it

https://doi.org/10.1016/j.xcrp.2021.100605

The protocol to convert fibroin into a bulk non-porous monolith has been known since the beginning of the 21st century[19,20,24,25] and has been proven to be versatile enough to be appliable, without major modifications, to different types of silk.[21] More recently, our group reported the possibility of performing the process at a lower temperature (40°C) by using starting material with a low amount of crystalline structures (β structures) and by the addition of water to decrease the glass transition temperature, thus allowing thermal reflow.[22] Starting from this protocol, complex architectures[23] that are suitable in non-structural applications in bone[26] have been produced. In fact, while the mechanical properties of solid silk were proven to be impressive in the dry state, in physiological conditions,[22,23] they were greatly reduced when the material was placed within, thus limiting the applications of this material.

This problem can be addressed by reinforcing SF through crosslinking, which can be achieved by creating either physical[27] or chemical[28,29] interactions among fibroin molecules. Physical crosslinking induces the transition of the protein secondary structure to the crystalline β form by chemical (i.e., ethanol, methanol, water vapor) or physical (i.e., shear stress, sonication) agents.[27] β Sheets are usually referred to as the reason for the impressive mechanical properties of the naturally spun silk fiber. In fact, they are closely packed and inflexible structures held together by intramolecular and intermolecular hydrogen bonds.[6] The increase in the β content allows one to maintain the mechanical stability in gels. Chemical crosslinking consists of the formation of covalent bonds between the protein chains, obtainable either by modifying the protein to add vinyl groups, which allows for a photoinduced chemical crosslinking[7,8,28–30] or by using naturally derived crosslinking agents that promote the formation of chemical bonds between reactive side groups on the protein chains, forming a continuous 3D network.[31–33]

Among these crosslinking agents, an interesting natural crosslinker for proteins is genipin, an aglycone derived from an iridoid glycoside called geniposide, which is also present in the fruit of *Gardenia jasminoides*.[34–36] The mechanism of crosslinking of genipin involves the reaction of amino acids with amines in their side groups. In case of fibroin, those side groups are mainly provided by lysine, which is present in small quantities (0.4%–1% mol, depending on the silk typology),[37–39] but still sufficient to ensure an effective crosslink of the protein. Although genipin is well known to be an effective crosslinker for fibroin, it has never been used to crosslink compression molded bulk fibroin for load-bearing applications.

In this study, we evaluated the impact on the solid silk properties of the exposure on physiological conditions. Thus, by an optimized protocol, we introduced genipin in the previously developed protocol, to obtain a solid SF monolith able to crosslink when exposed to the physiological condition. The process of compression was conducted at high temperatures to avoid the necessity of the addition of water and consequently the start of the crosslinking reaction.

To understand the effect of the process factors on the properties of the outcoming material, we adopted a response surface method (RSM). RMS is a statistical method used to model and optimize processes[40–46] in which more than one factor (process variable) is present. In RMS, the process is treated as a black box in which the controllable factors are set to strategic points of the factors' space to observe their effect on the yields of interest. Compared with the common approach of studying one factor at time (OFAT) versus one of the considered yields, RSM has the advantage of also considering how the interaction between factors affect the yields. This allows the development of empirical models, based on the observed datapoints, that not

only include, as terms of first order, all of the different factors but also, as terms of higher order, their mixed effects.[40]

An RSM has been used in combination with a compression test to maximize the Young's modulus of the material after 12 h in physiological conditions. The same method has been used in combination with Fourier transform infrared spectroscopy (FTIR) to determine the amount of β structures and to prove that the increase in the mechanical properties was not related to the increase in crystallinity but with the crosslinking action of genipin. Time-temperature superposition of the data generated by dynamic-mechanical thermal analysis (DMTA) allowed us to determine the variation of the storage modulus in dry conditions over an extended timescale (up to 1,000 years), proving a good stability in the case of dry conditions for both the crosslinked and the uncrosslinked material. While the crosslinking was fundamental, both to allow the partial recovery of the initial mechanical properties and to preserve the shape and the structural integrity during a prolonged degradation test in physiological conditions, complex structures were obtained by laser cutting, proving the versatility of the produced material. Finally, a preliminary biological evaluation was performed to ensure that the newly crosslinked material performs as well as the bare material produced by compression molding but without the addition of genipin.

RESULTS

Fabrication and evaluation of the chemical crosslinking

Although genipin is only slightly soluble in water, we were able to effectively add it to the fibroin water solution by the succession of steps illustrated in Figure 1A. We prepared a dispersion of genipin in water and mixed it to the cooled SF solution (at 4°C) to form a dispersion that was frozen with liquid nitrogen. This allowed us to avoid the crosslinking reaction to take place. After lyophilization and compression molding, we obtained a solid silk monolith with a uniform presence of genipin but still not crosslinked. The crosslinking took place when the solid silk was placed in physiological conditions (37°C, in water), as demonstrated by the change in color from golden and transparent to opaque violet (Figure 1B). The reaction kinetic was followed via the intensity of the visible spectrum at 620 nm (based on the collected spectra shown in Figure S1) that display a plateau after 12 h, regardless of the water bath temperature (25°C or 37°C). Therefore, a time interval of 12 h was used as the final time point for the compressive test.

The presence of genipin was further confirmed by several genipin-related peaks in the FTIR spectra of the crosslinked sample (XL) (Figure 1C). The peak at 1,104 cm^{-1} could be referred to both the ester group C-O-C in the genipin structure[47] and, in the case of the protein crosslinking, to the stretching vibration of C-N, where the atom N is the tertiary atom after the lysine reaction with genipin.[48] The peak at 889 cm^{-1} could be related to the C-H stretching vibration on the heterocyclic ring,[49] while the peaks at 768 and 796 cm^{-1} can be assigned to the C-H wagging of substituted aromatic rings.[50]

Even though the chemistry of the crosslinking reaction is still unclear, one of the most accepted pathways in the literature is reported in Figure 1D.[51,52] This reaction involves an initial nucleophilic attack of a primary amine group of the protein on the C3 carbon atom of genipin to form an intermediate aldehyde group. The opening of the dihydropyran ring is followed by an attack on the resulting aldehyde group by the secondary amine. This results in the closure of the ring and the loose of OH as leaving group. The subsequent alcohol dimerization, with the loss of water, builds the crosslinking bond between the fibroin chains.

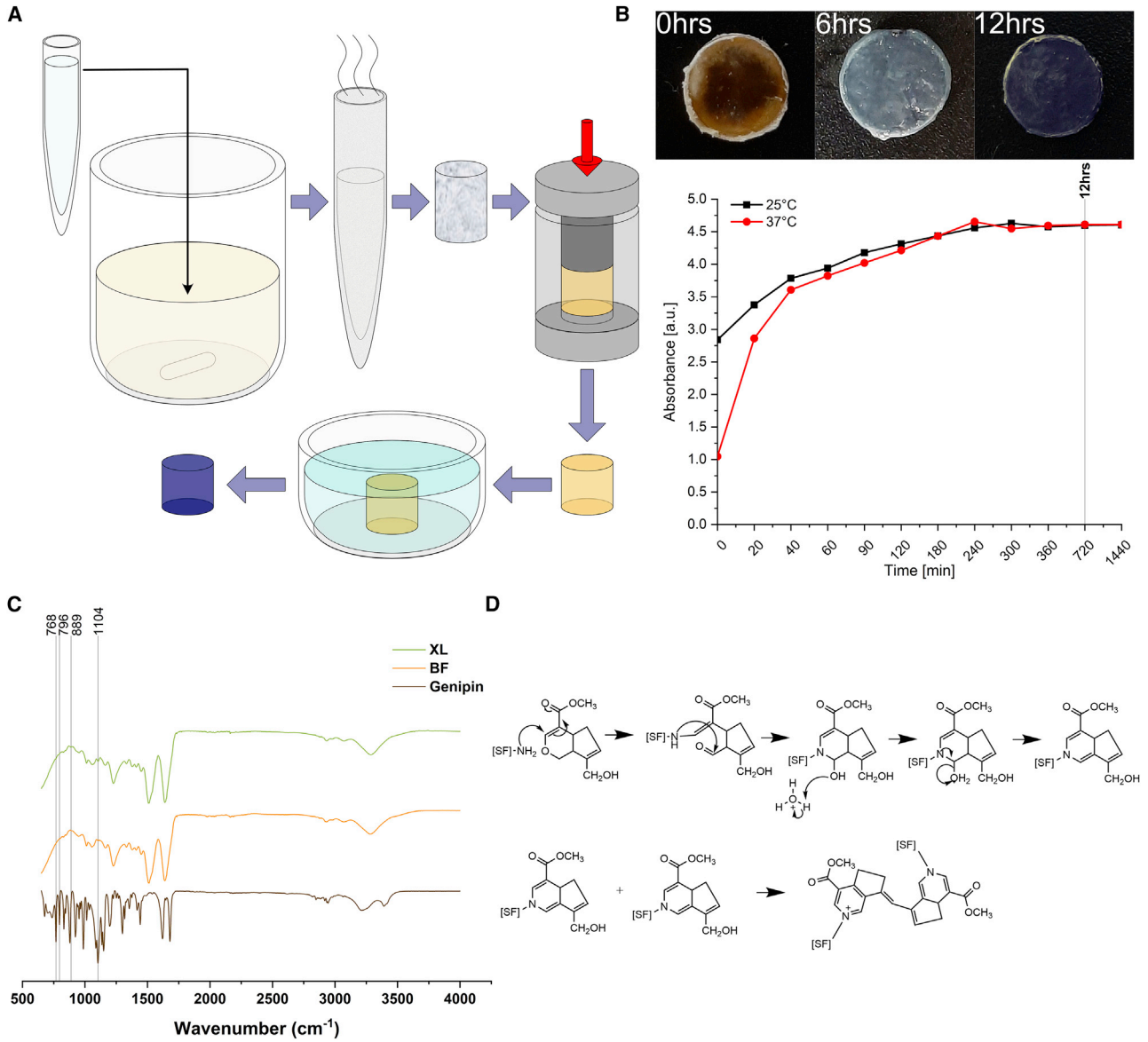

Figure 1. Scheme of the process and its chemistry

(A) Scheme of the process. To avoid any reaction in the fibroin solution, genipin is initially well mixed with water and subsequently rapidly mixed with the fibroin at 4°C. The solution is then frozen in liquid nitrogen and lyophilized. After the compression molding, we obtained a solid silk monolith with a uniform dispersion of genipin. The immersion of the monolith in water at 37°C allowed the crosslinking reaction.

(B) The crosslinking was followed by the intensity recorded at 620 nm of the visible spectra. In fact, during the crosslinking, the sample changed color to opaque violet. After 12 h, the intensity reached a plateau, and the reaction could be considered completed. It should be noted that both water temperatures tested gave the same results (the difference in the initial absorbance is due to the natural difference occurring in the samples; however, as soon as the crosslinking started, the absorbance became almost the same).

(C) FTIR spectrum of genipin, the monolith produced by only fibroin (BF), and the crosslinked monolith with 4% of genipin (4%XL). The presence of genipin was confirmed by several peaks in XL, not present in BF, and recognizable in genipin.

(D) Proposed crosslinking mechanism in the presence of water.

Mechanical characterizations and empirical modeling

The decrease in the compressive modulus in wet conditions was the major limitation of the previously proposed protocols to obtain bulk SF materials.[20,22,53] Genipin crosslinking allowed us to partially retain the pristine compressive modulus by avoiding plasticization of the material in wet conditions over time. The increase in the

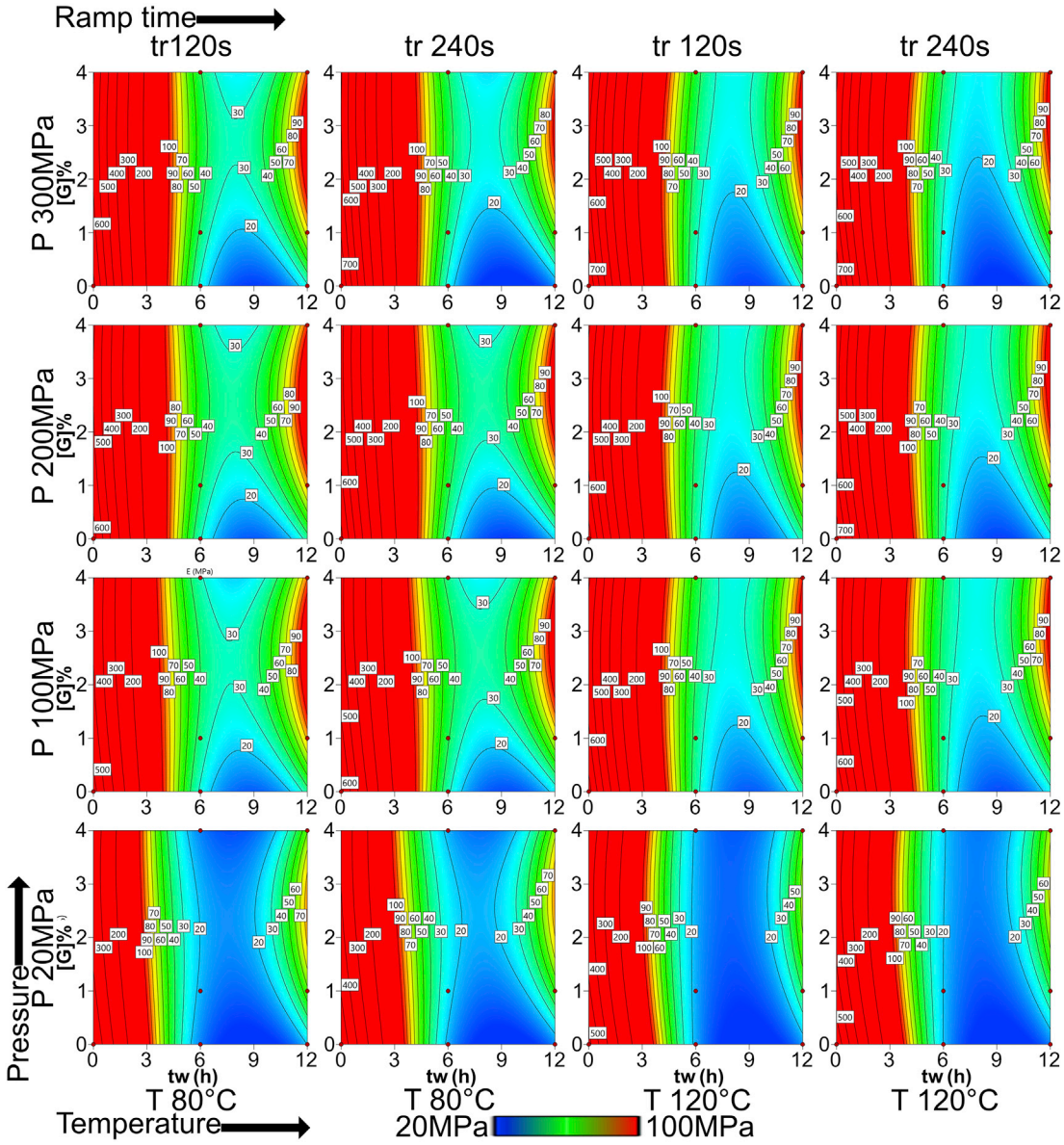

Figure 2. Contour plots of the modeled compressive modulus model

Each subpanel represents a specific process condition in which temperature, pressure, and ramp time were fixed, while within each panel the x axis represents the time in water at 37°C and the y axis the percentage of genipin added to the sample. The compressive modulus decreased with the time in physiological condition; the decrease began between 3 and 6 h and reached the minimum at >9 h. After 12 h, whenever no crosslinking was present, the modulus remained in the 20–30 MPa range, while it increased in the materials in which the genipin was added, reaching a maximum on the order of 100 MPa. A recovery zone was generated by the presence of a chemical crosslinking that allowed the partial restoration of the modulus. The red points indicate where the samples were made, and the data collected. The contours were not equally spaced. We reported 1 contour every 100 MPa in the 600–100 MPa range, and 1 contour every 10 MPa in the 100-0 MPa range.

mechanical strength after 12 h in water at 37°C is shown in Figure S3A, in which some selected stress-strain curves with an increase in the amount of genipin (from 0% of the bare fibroin [BF] to 4%) are presented. After 12 h in water, the increase in the amount of genipin was related to the increase in the compressive modulus. In Figure 2, the results of the empirical model of the compressive modulus are shown as multiple contour plots (complete statistical treatment in Tables S1 and S2 and

Figure S2). In each contour plot, the vertical axis reports the genipin content (0%–4%) and the horizontal axis reports the soaking time in water at 37°C before the mechanical tests (0–12 h). The other labels define the conditions of sample preparation in terms of temperature (*T*), pressure (*P*), and ramp time (*tr*). When genipin was not present, the compressive modulus strongly decreased with increasing soaking time, from 300 to 500 MPa of dry samples down to 20–30 MPa after 12 h soaking, regardless of the sample preparation conditions (bottom-right corner of each plot). Moving to higher genipin percentages, the compressive modulus first decreases with soaking time, but then it increased because of crosslinking, and after 12 h in pseudo-physiological conditions, the resulting modulus sometimes overcame 100 MPa. The recovery zone, in which the modulus increased, changed its position and extension depending on the conditions of sample preparation, but was always in the top-right corner, where the genipin percentage and soaking time allowed an efficient crosslinking. Considering a soaking time of 12 h, the compressive modulus increased with the genipin amount, but these trends almost always showed an inflection point, which indicates that there is an optimal genipin amount for each set of sample preparation conditions, above which the increment in the compressive modulus is marginal. Some general trends are appreciable by comparing the different plots. An increased applied pressure during sample preparation extended the zone with a compressive modulus >100 MPa (red zone) toward inferior soaking times and slightly increased the maximum modulus. However, the "weak" area with a modulus <20 MPa (blue zone) first contracted with increasing applied pressure, but then it expanded to a pressure of 300 MPa, which indicates the existence of an optimal applied pressure. The weak area was also smaller for lower temperatures and lower ramp times.

An additional statistical approach, called the desirability approach (Figure S2), was performed to maximize the compressive modulus by keeping the soaking time in pseudo-physiological conditions fixed at 12 h. This maximization resulted in a set of optimal process parameters (i.e., p = 160 MPa, *tr* = 120 s, *T* = 80°C, *[G]* = 2.6%). The compressive modulus was optimized to a value of 127 MPa, with an increment of 318% compared to that of genipin-free material in the same conditions (36 MPa).

DMTA tests were performed to study the viscoelastic properties on bars produced by compression molding of BF and crosslinked fibroin containing 4% of genipin (4%XL). Single-frequency tests (Figure 3A) revealed that, for both samples, the storage modulus (*E′*) decreased throughout the whole investigated temperature range and with a clear step at 140°C and 100°C for BF and 4%XL, respectively. The step was accompanied by multiple peaks in the signals of loss modulus (*E″*) and loss factor (*tanδ*), which demonstrated several high-temperature transitions. For BF, *tanδ* manifested three evident signals, attributable to the glass transition of dry fibroin and to the random coil-to-β sheet conformational transition.[54] More specifically, the random coil-to-β sheet transition is likely related to the highest-temperature peak; this transition leads to an increase in the fraction of stiff β sheet phase, and in fact, it is accompanied by an increase in *E′* > 180°C. For 4%XL, *tanδ* manifested 2 broad signals at 115°C and 190°C. The latter temperature was similar to what was reported for fibroin films treated with ethanol and attributed to the induced β sheet crystallization.[55] In that work, the high temperature peak was assigned to β sheet relaxation, while the low temperature peak (155°C) was attributed to the relaxation of uncrystallizable and permanently disordered domains with a higher free motility than β sheet domains. For BF, an additional transition was observable at ~−60°C, which is generally attributed to a fibroin-water complex glass transition[56] or to hydrocarbon

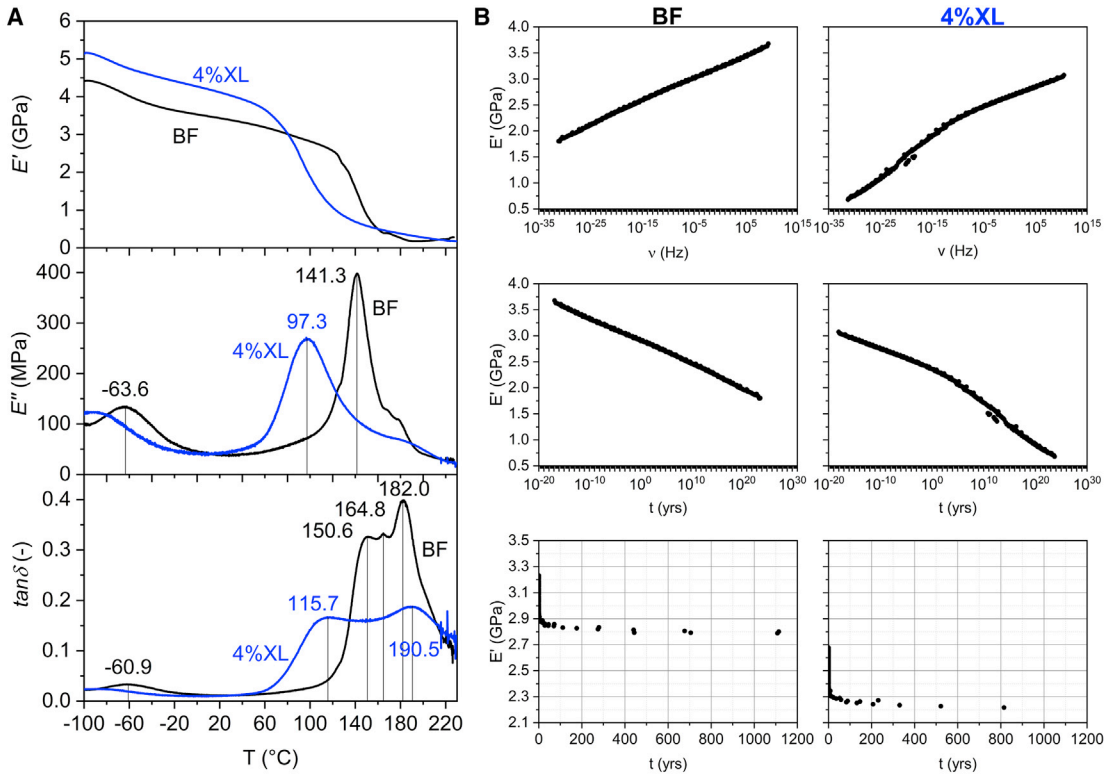

Figure 3. Results of dynamic-mechanical thermal analysis (DMTA)

(A) Single-frequency (1 Hz) DMTA tests on compression-molded samples of bare (BF) and crosslinked fibroin (4%XL) containing 4% of genipin. Storage modulus (E′), loss modulus (E″), and tanδ as a function of temperature. Numbers indicate peak temperatures.

(B) Master curve obtained in multifrequency DMTA tests. Complete master curves of E′ are reported as a function of frequency (first row) and time (second row), and detail of the time-dependent master curve is reported on linear scale up to 1,200 years (third row).

interactions.[57] At the end of the test, in both samples, the noise in the *tanδ* signal increased considerably, which was a sign of incipient thermal degradation, reported to occur above ~240°C.[55]

The viscoelastic properties were further interpreted by plotting *E″* as a function of *E′* (Figure S4A). This representation, called the Cole-Cole plot, resulted in an arc of a circle for both samples, although imperfect, which suggested that these materials could be regarded as homogeneous and thermorheologically simple.[58–60] This led us to apply the time-temperature superposition principle on multifrequency DMTA data (Figure S4B) to obtain a reliable master curve (Figure 3B). This approach gives information on the material behavior for very long times, thus estimating the material durability and long-term retainment of the mechanical properties. As expected, *E′* decreases over time. However, since the glass transition of bulk fibroin in the dry state was considerably higher than the service temperature, the predicted decrease in storage modulus was modest even after 1,000 years in both BF and 4% XL samples (Figure 2D, last row), even though in this test, BF showed a slightly higher storage modulus. This partially confirmed our previous model in which in a dry state, the compressive modulus was slightly higher for BF than for crosslinked fibroin, but this was inconsistent with the single-frequency DMTA test in which 4%XL had the highest *E′*, at least until 80°C. Since the *E′* value obtained for BF and 4%XL were not so different, we could hypothesize that this inconsistency resides in the natural variability of the material and of the process.

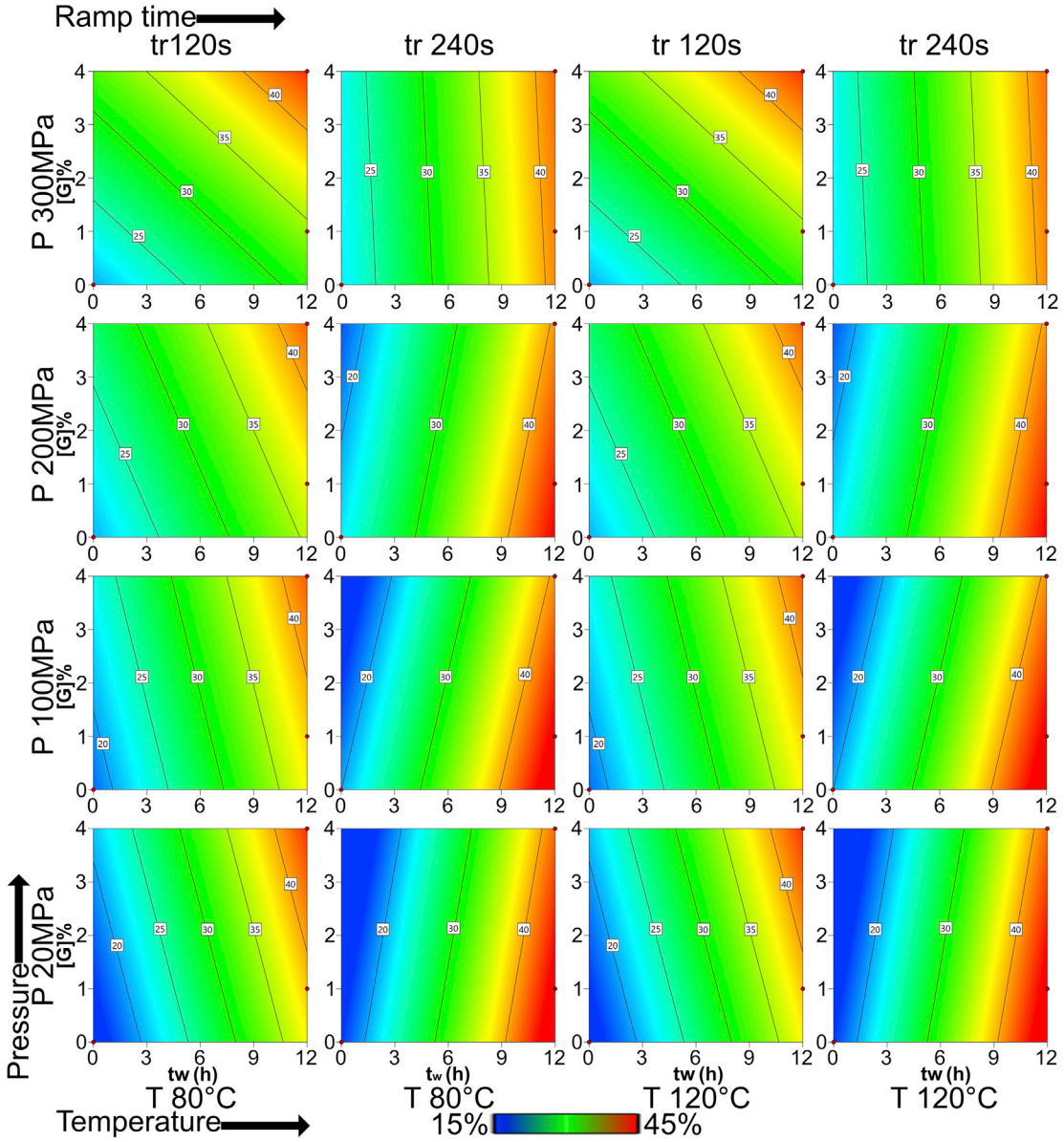

Figure 4. Contour plot of the modeled index of crystallinity

Each subpanel represents a specific process condition in which temperature, pressure, and ramp time were fixed, while within each panel, the x axis represents the time in water at 37°C and the y axis the percentage of genipin added to the sample. How could be expected the prolonged exposition to the physiological condition induced the transition of the secondary structure to the crystalline β sheet. Interestingly, we did not see any significant effect of the process temperature; however, this could be explained considering that the process was too fast to notice any effect over the time due to the temperature increase. The increase in the amount of genipin slightly increased the crystallinity only in the case of a fast application of the pressure (*tr* = 120 s) while in the other condition (*tr* = 240 s), a slight decrease was found.

Secondary structure and empirical modeling

The primary amide portion of the FTIR spectra was analyzed (1,580–1,720 cm^{-1}) to determine variations in the secondary structure. The sum of the percentage area occupied by the peaks related to the β structures (parallel and antiparallel) has been used as an index of crystallinity. This index has been modeled and the contour plots reported in Figure 4 (complete statistical treatment in Tables S3 and S4 and Figure S5). In contrast to other works on the topic, the process temperature did

not statistically influence the amount of crystallinity. However, our process was extremely fast, lasting from 2 to 4 min, thus probably not sufficient to induce the protein crystallization. Based on the compressive ramp, the presence of genipin slightly changed the crystallinity. In particular, with the faster pressure ramp (120 s), the increase in the amount of genipin increased the amount of β phases, while with the slower pressure ramp (240 s), the trend was reversed and less marked. As expected, the crystallinity of the samples increased by the increment of the time passed in physiological conditions (t_w) of the samples soaked in water because of the material plasticization.

Interestingly, by comparing the contour plot of the crystallinity with the results obtained from the compressive modulus (Figure 1), we could conclude that the increment in the compressive modulus observed was not related to the crystallization, thus confirming the role of the chemical crosslinking. In fact, the difference in the crystallinity between the sample with genipin (*[G]* = 2.6%) and without genipin in the condition in which the compressive modulus was maximized (p = 160 MPa, *tr* = 120 s, *T* = 80°C) was estimated at 3%, which is not sufficient to explain the increment in the compressive modulus. It should be noted that the lower intensity of the signal of the crosslinked sample (4%XL) obtained in the transitions revealed by DMTA (*tanδ*; Figure 2A) is in accordance with its highest amount of the β structures, as compared with the sample without genipin (BF).

Degradation and shape retention in physiological conditions

The long-term behavior of the crosslinked material was also investigated in physiological conditions by a degradation test within the enzymatic action of a protease (Figure 5). The results confirmed the action of the crosslinking effect of genipin that allowed the retention of the structural integrity of the samples for the entire month of testing, while samples prepared in the same conditions but without genipin lost their original shape and integrity. The reason behind this improvement was revealed by observing the degradation mechanism (Figure 5A). In fact, compression molding resulted in a layered microstructure, with cavities among the layers. These cavities tended to swell by the penetrated testing medium, and this strongly compromises the structural integrity of the samples. This effect is considerably less clear on crosslinked samples, probably due to the enhanced chemical bonding in between the layers. This effect was even more striking when the percentage of protease was increased to boost the degradation rate. After 1 day (last column of Figure 5A), the sample without genipin was severely cracked, while the sample with 4% of genipin was still intact.

The swelling ratio (Figure 5B) reached a plateau after the first time point, regardless of the sample. The plateau was higher for the group of uncrosslinked samples in comparison with the group of the crosslinked samples, and in each group, it was higher for the sample produced at 80°C in comparison with the sample produced at 120°C. The swelling ratio was in the 35%–55% range, the maximum value reached after 30 days was 54.4% ± 1.9% (BF 80°C), and the minimum 3.6% ± 0.1% (4%XL 120°C). The range was lower compared to the usual swelling found in fibroin scaffold, confirming the non-porous nature of the material, but still higher than the common swelling ratio of polymers, demonstrating that the material was permeable to water.

The degradation rate, reported in Figure 5C, was higher for the group of uncrosslinked (BF) samples compared to the crosslinked samples (4%XL) and, within each group, higher for the samples prepared at a lower temperature (80°C). In

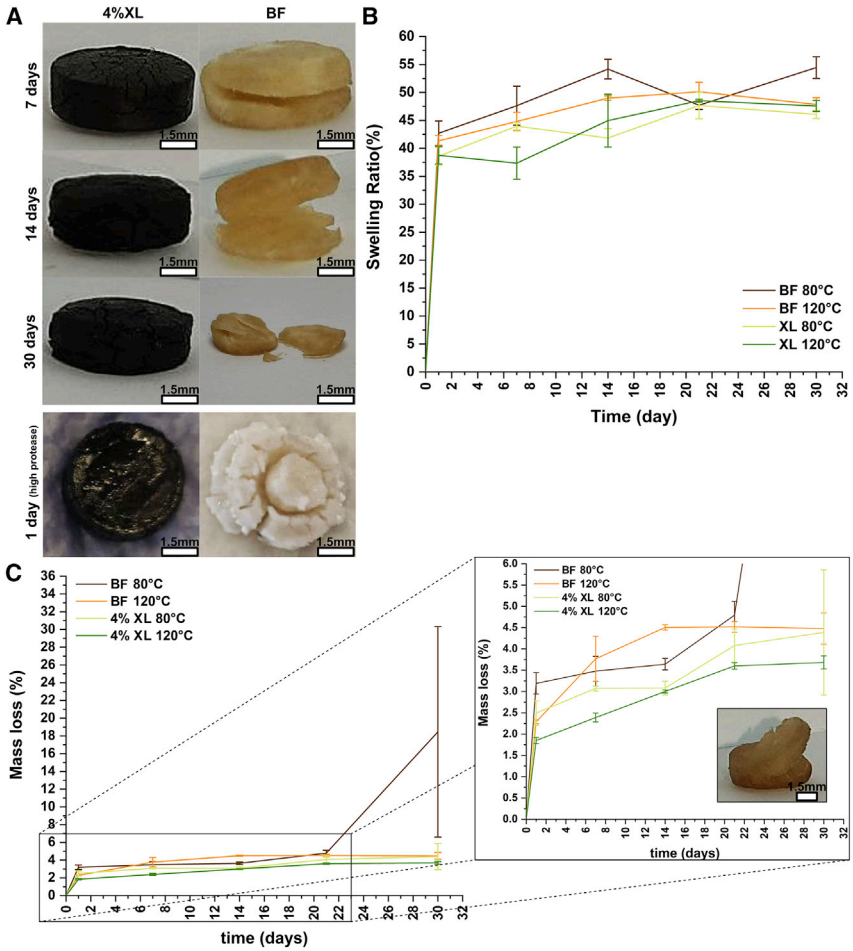

Figure 5. Sample degradation, swelling ratio, and mass loss in enzymatic solution at 37°C

(A) Picture of the samples prepared at 80°C after 7, 14, and 30 days in physiological conditions, and after 1 day in physiological conditions with a high concentration of protease. Overall, the crosslinked samples (4%XL) were able to maintain their original shape and integrity, while the uncrosslinked samples did not. At the time point, the BF sample was broken in pieces. Scale bar, 1,500 μm.

(B) The swelling ratio was dependent on both the crosslinking and the temperature. However, at the last day, all of the samples had a swelling ratio between 35% and 55%, indicating a non-porous material.

(C) All of the samples, with the exclusion of BF 80°C, had a mass loss between 3% and 5%. BF 80°C due to the breakdown had a much larger mass loss. It should be noted that even if BF 120°C lost 5% at day 30, the sample would totally lose its initial shape, as can be seen. Scale bar, 1,500 μm.

particular, at the end of the 30 days, the sample with the lowest mass loss was that produced at 120°C crosslinked with 4% of genipin (4%XL 120°C), while the most degraded sample was that produced at 80°C without genipin (BF 80°C). This latter, in the last 9 days of the test, was disintegrated into multiple pieces, while the sample produced with BF but at a higher temperature (BF 120°C) lost its shape but remained in a single piece. Excluding the last time point, all of the samples had the highest decrease in weight during the first 24 h. After the first time point, the rate of weight loss became slower, as observed from the magnification of Figure 5C. The lower mass loss after 30 days was 3.68% ± 0.15% obtained with the crosslinked samples produced at 120°C (4%XL 120°C), while the maximum was 18.4% ± 11.8% of the broken uncrosslinked samples produced at 80°C (BF 80°C).

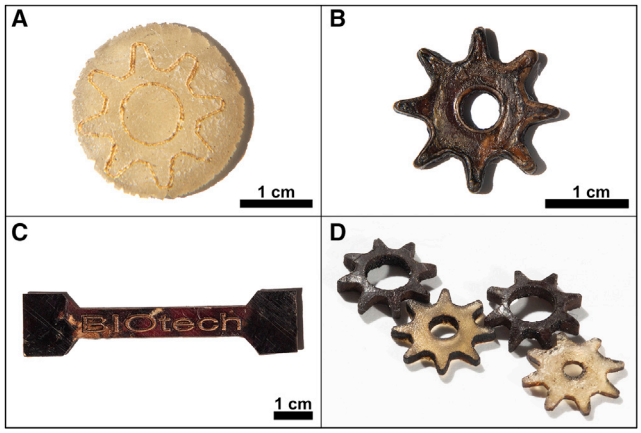

Figure 6. Object obtained by laser cutting, starting from a thin cylinder of molded silk

(A) Thin cylinder in the first phase of the laser cutting. Scale bar, 1 cm.

(B) Crosslinked cylinder with 4% of genipin cut in the shape of a gear. Scale bar, 1 cm.

(C) Dumbbell with engraving. Scale bar, 1 cm.

(D) Composition of different gears with different thickness and internal cut.

Shaping by laser cutting

As proof of concept, we demonstrated the possibility of developing complex shapes by producing plates of solid silk and then cutting it with a laser. Three sets of conditions of the laser cutter were tested with different power and velocity (Figure S6); the best one was chosen to produce the objects shown in Figure 6. The laser cutting required to run the laser over the same path multiple times to achieve reliable reproduction in a single run is shown in Figure 6A. We were able to cut effectively both the solid material from the BF and the crosslinked material (Figures 6B–6D). In addition, in choosing the appropriate power level, it is possible to engrave figures in the material. For example, in Figure 6C, we engraved characters on a dumbbell for the tensile test.

Evaluation of cell adhesion and proliferation through *in vitro* confocal imaging

A preliminary *in vitro* biological evaluation allowed us to compare the material produced with this novel protocol with the bare material produced in the same conditions, but without the addition of genipin. The confocal images obtained are shown in Figure 7. Human bone marrow mesenchymal stem cells were studied in both samples. After 10 days of culture, the cytoskeleton was stained with Oregon Green and observed. DAPI was completely absorbed by the substrates and was not visible in the micrographs due to the strong background (Figures 7A and 7B). In both cases, the cells showed good adhesion to the substrates and no visible differences in their morphology. However, 4%XL showed a slight increase in the degree of cell spread if compared with the BF formulation. Compared with the BF sintered substrate (BF; Figure 7A), the crosslinked sample (4%XL; Figure 7A) had slightly lower cell density and distribution. However, the performances of the substrates were almost comparable. This seems to be in contrast to a previous study in which genipin was reported to be cytotoxic.[61] Being the first time that genipin has been used in a solid bulk material, the previous results are difficult to compare to our trial. We hypothesized that the effect of genipin may be mitigated by the solid matrix that slows down its release in the environment. The cells were also cultivated on a large, crosslinked gear-shaped sample (Figure 7B), and in this case, the cells adhered to the substrate.

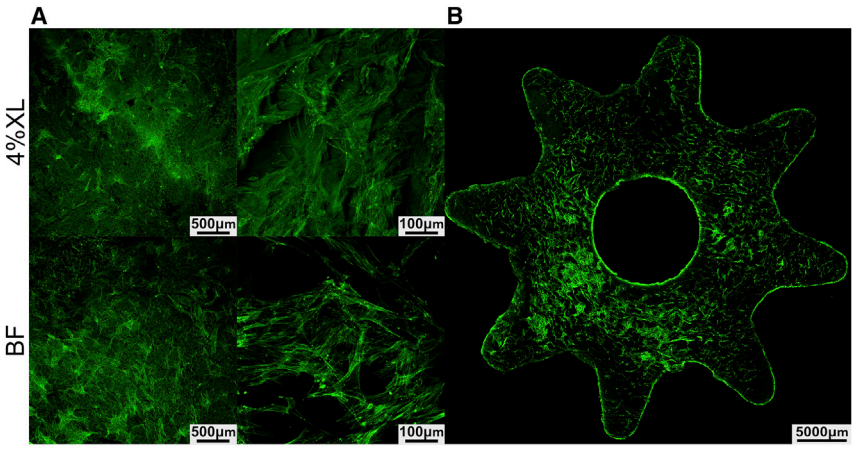

Figure 7. Confocal imaging on cell-cultured silk monoliths

(A) Comparison between the crosslinked fibroin with 4% of genipin (4%XL) and the bare material (BF) at 2 levels of magnification. Scale bars, 500 µm (first column), 100 µm (second column).

(B) Cell seeded on the crosslinked gear obtained by laser cutting (see Figure 6B). Scale bar, 5000 µm.

DISCUSSION

A strategy to produce solid crosslinked fibroin has been developed by adding genipin and successively crosslinking in water at 37°C. We proved that this material in physiological conditions after an initial decrease in the compressive modulus begins to recover by the effect of the ongoing crosslinking reaction, while in the material produced without genipin, it showed a progressive decrease in the modulus over time. The increase in the compressive modulus of the crosslinked material could not be ascribed to the increase in the crystallinity that took place in both samples with and without genipin. The crosslinking was proven by the changing of the color from golden transparent to violet opaque, revealed also by the increase in intensity at 620 nm in the visible spectra. The comparison with the material prepared in the same condition but without genipin revealed that the crosslinking allowed us to preserve the mechanical integrity and the shape of the object during a degradation test with protease, while the uncrosslinked material after 30 days showed evident opened fractures. Complex objects were produced by laser cutting, proving the versatility of the crosslinked material that was machinable as the uncrosslinked. The preliminary biological test revealed that the crosslinked material, after 10 days of incubation, were not significantly different, in cell adhesion and proliferation, from the material produced without genipin. In summary, crosslinked solid fibroin solved the issues due to the previously reported protocols, and due to its properties, it is suitable for structural applications in physiological conditions that require reliability in the mechanical performance and stability in shape. Based on this proof of concept, complicated objects such as screws and bars may be produced to substitute materials used in bone surgical procedures; this would avoid the necessity of the extraction of the material after the complete recovery thanks to its slow resorption. In addition, the same procedure may be used with other biopolymers to produce a family of structural materials, allowing us to adapt the type of material to specific surgical needs.

EXPERIMENTAL PROCEDURES

Resource availability

Lead contact

Further information and requests for resources should be directed to and will be fulfilled by the lead contact, Alessio Bucciarelli (alessio.bucciarelli@nanotec.cnr.it).

Materials availability

This study did not generate new unique reagents.

Data and code availability

All of the data reported in this article are available from the lead contact upon request.

Fabrication of the bulk crosslinked SF

Degummed SF has been obtained by a modified version of a well-established protocol.[12] Briefly the cocoons (imported from Chul Thai Silk, Thailand) were cut in pieces and placed in a 0.01-M hot bath of sodium carbonate (Na_2 CO_3, Sigma-Aldrich, USA) for 1 h, followed by a second immersion in a bath with a concentration of 0.003 M for 1 h. The resultant SF, progressively taken at room temperature, was carefully rinsed 3 times using ultra-pure water and then dried for 2 days. The resulting degummed SF was dissolved into a 9.3-M water solution of lithium bromide (Sigma-Aldrich) at 60°C for 4 h in a 2 g/10 mL concentration. Once SF was dissolved, the solution was taken at room temperature and then dialyzed against water for 3 days in a dialysis tube (cutting M_w = 3 kDa) to remove the salt. The concentration of the fibroin solutions was determined by the use of the protein absorbance peak at 280 nm using a Nanodrop UV spectrophotometer (Thermoscientific, USA). From this quantity, the amount of genipin to dissolve into the SF solution has been calculated using Equation 1, where [G] is the percentage concentration (w/w of SF) on of genipin that we aimed to obtain, V_{SF} is the volume of SF solution, and [SF] is the concentration of fibroin in milligrams per milliliter. To rapidly dissolve the genipin inside the fibroin solution, avoiding the crosslinking reaction, a mother solution of genipin was prepared with a known concentration and subsequently added to the SF solution and stirred for a few minutes at 4°C, to reach the desired genipin:fibroin weight ratio. The prepared solutions were then rapidly frozen with liquid nitrogen and freeze-dried at −50°C until the water was completely removed. The obtained fibroin-genipin sponges were maintained in dry conditions at 4°C to avoid the crosslinking reaction. The solid samples were prepared by placing a 200-mg sponge into a cylindrical mold with a diameter of 6 mm and using a universal testing machine (MTS 858 Mini Bionix, Italy) within an integrated oven that allowed us to set the process temperature within a range of ±1°C. Once the process temperature was reached, a compression ramp was applied to reach the desired force (*F (kN)*) in the desired time (*tr(s)*). The results were cylinders with a thickness of ~5 mm. The bulk fibroin cylinders were finally placed in water at 37°C ± 1°C for a variable time to simulate the physiological condition and to allow the crosslinking reaction to take place. A change from the transparent yellowish color to violet opaque was observed, indicating the successful crosslinking reaction. We compared this material to the equivalent material prepared from the bare SF without the addition of genipin. The entire fabrication process is presented in Figure 1A. Using the same method, with different molds, bars with a dimension of 40 × 5 mm and a thickness of 2 mm and cylinders with a diameter of 30 mm and a thickness of 2 mm were prepared.

$$m_G(mg) = [G]V_{SF}[SF] \qquad \text{(Equation 1)}$$

Structural characterization

The crosslinking reaction was followed by an evaluation of the intensity of the UV-visible (UV-vis) spectra (Jasco V-570 spectrophotometer, USA) on a single wavelength (620 nm) related to the transition to a violet color of genipin due to the crosslinking.[62] Two conditions were tested: crosslinking in water at 25°C and at 37°C. The secondary structure changes were evaluated using an attenuated total reflectance FTIR (ATR-FTIR) spectrophotometer (Perkin Elmer Spectrum ONE, USA). To maximize the signal-to-noise ratio, 32 spectra with a resolution of 1 cm^{-1} were collected and averaged for each sample. The SF secondary structures were then quantitatively

evaluated by analyzing the primary amide peak (1,580–1,720 cm^{-1}). The methodology is briefly illustrated in Figure S7. The peak was smoothed with a 5-point adjacent averaging function followed by a Fourier self-deconvolution (with a smoothing factor of 0.3 and gamma function of 30) to enhance the resolution and better shape the singular components. A second derivative was then performed to identify the peak position. These values were then used to fit the single peaks with a Gaussian function. The fitting routine was recursively applied until χ^2 was minimized. The ratio between the fitted peak area and the total area was calculated to determine the percentage of the specific structure assigned to the peak.[63,64] In Table S5, the assigned secondary structures for different bandwidths of the FTIR spectrum are reported. We tested a single sample for each of the conditions listed in Table S6.

Mechanical characterization

Compression tests were performed on the samples produced following Table S6 using an Instron 7500 universal testing machine (USA) with a compression rate of 1 mm/min in a controlled environment (25°C and 20% relative humidity). A precompression of 0.2 kN was applied pre-testing. The Young's modulus (E) was evaluated as the angular coefficient of the curve in the initial elastic (linear) zone. The test was conducted in dry conditions or just after the soaking in water at 37°C for the predetermined time (6 or 12 h). On these results, a statistical method was applied to maximize E after 12 h in water. To verify the effect of the crosslinking agent, a sample with genipin (4%) was tested versus a reference sample (without genipin) by DMTA (TA Q800DMA, USA) conducted on bars using a single cantilever bending mode (span = 17.5 mm). The specimens were in the dry state and in the form of bars with a rectangular cross-section with nominal dimensions of 40 × 5 × 2 mm. Both samples were prepared by compression at 120°C with a maximal pressure of 343 MPa reached in a ramp time of 120 s. In this test, the samples were nominated as BF and 4%XL. E', E'', and $tan\delta$ were determined between −100°C and 230°C, at a heating rate of 3°C/min, a strain amplitude of 0.05%, and a frequency of 1 Hz (single-frequency tests). In addition, multifrequency tests were carried out in the same testing configuration between 0°C and 190°C, at a heating rate of 0.2°C/min. The 11 investigated frequency levels (Hz) are 0.50, 0.79, 1.30, 2.00, 3.20, 5.00, 7.90, 12.60, 19.80, 31.50, and 50.00. To build the master curve, data were shifted automatically with the software TA Rheology Advantage (TA Instruments, USA), keeping a reference temperature of 23°C. In this way, E' can be determined in a wide frequency interval, which ranges from 10 to 32 to 108 Hz. These data were then used to build a durability curve by transforming the values of frequencies (Hz) in values of time (years). For the purpose of the present analysis, the data of durability were of interest in a time frame between 1 s (3.2×10^{-8} years) and 1,000 years.

Degradation

The study of degradation is performed over 2 kinds of material BSF and GXSF4, all sintered at 300 MPa—half at 80°C and half at 120°C—for a total amount of 80 samples. Samples were left to degrade in a solution simulating a physiological condition. The solution was prepared with phosphate-buffered saline (PBS), pH = 7.4 (Sigma-Aldrich), with the addition of protease XIV (Sigma-Aldrich), with a concentration of 0.2 mg/mL, to achieve an enzymatic action. To accelerate the degradation, we used 1 mg/mL protease XIV. Then, sodium azide (Sigma-Aldrich), with a concentration of 0.04 mg/mL was added to avoid bacteria proliferation. Even if the use of a single enzyme is not comparable with a biological system in which multiple phenomena occur, protease XIV being effective in accelerating the degradation of SF has been widely adopted in the literature.[65,66] Despite its limited clinical value, the degradation test with protease XIV can clearly reveal general trends of the material

behavior exposed to an enzymatic environment closer to a biological environment if compared with the only use of PBS. As reference, we prepared a control solution of PBS, with the same concentration of sodium azide. The samples were placed in multiwells, 2 mL of solution each, and stored at 37°C. The mass of the samples before and after the degradation was recorded (analytical balance Kern Abs-N, UK). Three samples for each time point for each condition were tested for a total of 80 samples. All of the samples underwent an initial incubation (BINDER, Germany) in deionized water for 6 h at 37°C and subsequently dried for 7 days in an oven (G-Therm, Italy) at 65°C. The initial weight was then recorded (m_0). The samples were allowed to degrade. At each time point (1, 7, 14, 21, and 30 days), 3 samples for each condition were taken out of the solution, briefly dried with absorbent paper, and weighed (m_{wet}). Then, after the removal of all of the water (in oven, 7 days, 65°C), the samples were weighed again (m_{dry}) and then trashed. Equation 2 has been used to calculate the mass loss, and Equation 3 has been used to calculate the swelling ratio.

$$\Delta m(\%) = \frac{m_{dry} - m_0}{m_0} * 100 \qquad \text{(Equation 2)}$$

$$Sw(\%) = \frac{m_{wet} - m_{dry}}{m_{dry}} * 100 \qquad \text{(Equation 3)}$$

Laser cutting

Laser cutting was conducted on the large cylinders (30 mm diameter) as a proof of concept of the ability to form this material into different shapes. The model was drawn using an open access vectorial software (InkScape) and cut into the material using a 30-W CO_2 laser cutter (Speedy 100R, Trotec, Italy) with a level power of 4 (12 W) and speed of 0.9 mm/min (both parameters of the machines without a reference unit), a frequency of 1,000 Hz, and 200 layers of cut, for a 20 min total process.

In vitro preliminary evaluation

Samples were washed in deionized (DI) water and then soaked in a 75% ethanol solution for 30 min, and rinsed 3 times in DI water to remove the ethanol. Human bone marrow mesenchymal stem cells (hMSCs, ATCC, PCS-500-102) were used in this study. The cells were cultured in the Dulbecco's modified Eagle's medium/nutrient mixture F-12 (DMEM/F-12) with 10% fetal bovine serum (FBS), and 1% antibiotic/antimycotic. The cells were cultured in a T75 flask at 37°C with 5% CO_2 in a humidified atmosphere. The cells were fed every 2 days until the cells reached 70% confluence. The cells (at passage 2) were detached from the flask by 1% trypsin-EDTA solution, re-suspended in standard medium, and seeded in a 24-well plate (40,000 cells/well in 0.8 mL medium) with the samples inside. The medium was changed every 2 days. Cell adhesion was visualized by Oregon Green phalloidin and 4′,6-diamidino-2-phenylindole (DAPI) staining on sintered SF substrates with and without genipin crosslinking. Oregon Green phalloidin stains the cytoskeleton, resulting in green fluorescence, while DAPI stains nuclei, resulting in blue fluorescence. After 10 days of culture, the cell-seeded samples were fixed with 4% paraformaldehyde, washed 3 times with PBS, and then permeabilized using 0.1% Triton X-100 PBS solution for 30 min. After washing in PBS 3 times (15 min each time), cells were incubated with Oregon Green phalloidin (5.0 μL/well) and DAPI (1.0 mL/well, 5.4 μL dilute in 25.0 mL PBS) for 45 min at room temperature. After three rinses with PBS, samples were observed by confocal microscopy (Nikon-A1, USA). It should be noted that colorimetric methods to assert the cell viability were not suitable in this specific case. In fact, the release of the crosslinked protein modifies the color of the cell medium and the surrounding environment, making colorimetric measurements unreliable.

Table 1. Tested factors within their levels

Factor name	Factor code	Measurement unit	Levels
Force	(A) F	kN	1, 5, 10, 15
Ramp time	(B) t_r	s	120, 240
Time soaked in water	(C) t_w	h	0, 6, 12
Temperature	(D) T	°C	80, 120
Genipin concentration	(E) [G]	% w/w	0, 1, 4

A subset of the combinations of the of the factor levels listed in the table were chosen to allow us to develop a reliable model for both the Young's modulus and the crystallinity index. Each point of this subset is shown in the contour plots as a red dot.

Statistical methods

The entire statistical analysis has been done in the programming language R[67] following the statistical strategy described in previous works.[22,30,68,69] An initial comparison to verify the presence of significant difference among the different groups was performed using analysis of variance (ANOVA), followed by a Tukey multi-comparison test. The significance levels were assigned as follows $p \leq\leq 0.1$ (.), $p \leq 0.05$ (*), $p \leq 0.01$ (**), and $p \leq 0.001$ (***). A RMS been adopted to model the empirical equations relating the considered process factors to the yields. These methods allowed us to understand the most significant terms and to separate them from the insignificant ones. Here, we considered five continuous factors. For each of them, we decided on a number of levels according to what we discovered from our previous work about their importance.[22] In Table 1, the considered factors within their level are listed, while the complete list of trials is reported in Table S6. Only a subset of the possible combinations has been tested. In particular, 108 combinations have been chosen and for each of them, 3 samples were prepared and tested. Only the significant terms were included in the models; an ANOVA test followed by a Tukey multi-comparison were conducted to verify their significance, and only terms with a $p \geq 0.01$ were included. A function F has been applied to the yield, when necessary, to both normalize the model residues and to make them pattern less. The model was considered significant, with a $p \leq 0.05$. The coefficient of determination (r^2) was calculated to determine the goodness of fit of the model. Models with a perfect fitting have a $r^2 = 1$. The optimization has been done by a numerical method based on desirability functions. These functions are in the [1,0] range, where 1 represents the optimum solution. One of these functions was assigned to each of the considered yields. We used the following notation: Y_i, the specific yield, d_i, the corresponding desirability function, and U_i and L_i, the maximum and the minimum value of the yield, respectively. For the maximization of Y_i, the function is reported in Equation 4; for the minimization, the function is reported in Equation 5. The overall desirability is the geometric mean of all of these functions reported in Equation 6, with k equal to the total number of yields (in our case, 2). Then, D is plotted against the process factors to find its maximum value and thus the best solution:

$$d_i = \begin{cases} 1 & if\ Y_i \geq U_i \\ \dfrac{Y_i - L_i}{U_i - L_i} & if\ L_i \geq Y_i \geq U_i \\ 0 & if\ Y_i \leq L_i \end{cases} \qquad \text{(Equation 4)}$$

$$d_i = \begin{cases} 0 & if\ Y_i \geq U_i \\ \dfrac{Y_i - L_i}{U_i - L_i} & if\ L_i \geq Y_i \geq U_i \\ 1 & if\ Y_i \leq L_i \end{cases} \qquad \text{(Equation 5)}$$

$$D = (d_1 d_2 d_3 \ldots d_k)^{\frac{1}{k}} \quad \text{(Equation 6)}$$

SUPPLEMENTAL INFORMATION

Supplemental information can be found online at https://doi.org/10.1016/j.xcrp.2021.100605.

ACKNOWLEDGMENTS

The project leading to this application received funding from the European Union's Horizon 2020 Research and Innovation Staff Exchange programme (RISE) under the Marie Skłodowska-Curie grant agreement MSCA-RISE 778078 (REMIX project). This research has also been supported by the Italian Ministry for Education, University and Research (MIUR) through the Departments of Excellence and the Regenera Project.

AUTHOR CONTRIBUTIONS

A.B. conceived the idea and the overall experimental planning, analyzed the data, and wrote the manuscript. V.J. prepared the samples and performed the mechanical testing. Y.Y. performed the cell culture and collected the confocal images. G.F. performed the dynamic mechanical thermal analysis. A.P., A.M., and D.M. supervised all of the work. All of the authors contributed to the revision of the manuscript.

DECLARATION OF INTERESTS

The authors declare no competing interests.

INCLUSION AND DIVERSITY

One or more of the authors of this paper self-identifies as a member of the LGBTQ+ community. One or more of the authors of this paper received support from a program designed to increase minority representation in science. While citing references scientifically relevant for this work, we also actively worked to promote gender balance in our reference list.

Received: July 11, 2021
Revised: September 4, 2021
Accepted: September 20, 2021
Published: October 8, 2021

REFERENCES

1. Kasoju, N., and Bora, U. (2012). Silk fibroin in tissue engineering. Adv. Healthc. Mater. *1*, 393–412.

2. Kundu, B., Rajkhowa, R., Kundu, S.C., and Wang, X. (2013). Silk fibroin biomaterials for tissue regenerations. Adv. Drug Deliv. Rev. *65*, 457–470.

3. Bhattacharjee, P., Kundu, B., Naskar, D., Kim, H.-W., Maiti, T.K., Bhattacharya, D., and Kundu, S.C. (2017). Silk scaffolds in bone tissue engineering: an overview. Acta Biomater. *63*, 1–17.

4. Holland, C., Numata, K., Rnjak-Kovacina, J., and Seib, F.P. (2019). The Biomedical Use of Silk: Past, Present, Future. Adv. Healthc. Mater. *8*, e1800465.

5. Wang, Y., Rudym, D.D., Walsh, A., Abrahamsen, L., Kim, H.-J., Kim, H.S., Kirker-Head, C., and Kaplan, D.L. (2008). In vivo degradation of three-dimensional silk fibroin scaffolds. Biomaterials *29*, 3415–3428.

6. Koh, L.D., Cheng, Y., Teng, C.P., Khin, Y.W., Loh, X.J., Tee, S.Y., Low, M., Ye, E., Yu, H.D., Zhang, Y.W., et al. (2015). Structures, mechanical properties and applications of silk fibroin materials. Prog. Polym. Sci. *46*, 86–110.

7. Bucciarelli, A., Mulloni, V., Maniglio, D., Pal, R.K., Yadavalli, V.K., Motta, A., and Quaranta, A. (2018). A comparative study of the refractive index of silk protein thin films towards biomaterial based optical devices. Opt. Mater. (Amst) *78*, 407–414.

8. Bucciarelli, A., Pal, R.K., Maniglio, D., Quaranta, A., Mulloni, V., Motta, A., and Yadavalli, V.K. (2017). Fabrication of Nanoscale Patternable Films of Silk Fibroin Using Benign Solvents. Macromol. Mater. Eng. *302*, 1700110.

9. Mitropoulos, A.N., Marelli, B., Ghezzi, C.E., Applegate, M.B., Partlow, B.P., Kaplan, D.L., and Omenetto, F.G. (2015). Transparent, Nanostructured Silk Fibroin Hydrogels with Tunable Mechanical Properties. ACS Biomater. Sci. Eng. *1*, 964–970.

10. da Silva, R.R., Cavicchioli, M., Lima, L.R., Otoni, C.G., Barud, H.S., Santagneli, S.H., Tercjak, A., Amaral, A.C., Carvalho, R.A., and Ribeiro, S.J.L. (2017). Fabrication of Biocompatible, Functional, and Transparent Hybrid Films Based on Silk Fibroin and Epoxy Silane for Biophotonics. ACS Appl. Mater. Interfaces *9*, 27905–27917.

11. Zhou, Z., Shi, Z., Cai, X., Zhang, S., Corder, S.G., Li, X., Zhang, Y., Zhang, G., Chen, L., Liu, M., et al. (2017). The Use of Functionalized Silk Fibroin Films as a Platform for Optical

Diffraction-Based Sensing Applications. Adv. Mater. *29*, 1–7.

12. Rockwood, D.N., Preda, R.C., Yücel, T., Wang, X., Lovett, M.L., and Kaplan, D.L. (2011). Materials fabrication from Bombyx mori silk fibroin. Nat. Protoc. *6*, 1612–1631.

13. Bai, S., Han, H., Huang, X., Xu, W., Kaplan, D.L., Zhu, H., and Lu, Q. (2015). Silk scaffolds with tunable mechanical capability for cell differentiation. Acta Biomater. *20*, 22–31.

14. Mandal, B.B., Grinberg, A., Gil, E.S., Panilaitis, B., and Kaplan, D.L. (2012). High-strength silk protein scaffolds for bone repair. Proc. Natl. Acad. Sci. USA *109*, 7699–7704.

15. Cho, H.H., Been, S.Y., Kim, W.Y., Choi, J.M., Choi, J.H., Song, C.U., Song, J.E., Bucciarelli, A., and Khang, G. (2021). Comparative Study on the Effect of the Different Harvesting Sources of Demineralized Bone Particles on the Bone Regeneration of a Composite Gellan Gum Scaffold for Bone Tissue Engineering Applications. ACS Appl. Bio Mater. *4*, 1900–1911.

16. Rajkhowa, R., Gil, E.S., Kluge, J., Numata, K., Wang, L., Wang, X., and Kaplan, D.L. (2010). Reinforcing silk scaffolds with silk particles. Macromol. Biosci. *10*, 599–611.

17. Yodmuang, S., McNamara, S.L., Nover, A.B., Mandal, B.B., Agarwal, M., Kelly, T.-A.N., Chao, P.H., Hung, C., Kaplan, D.L., and Vunjak-Novakovic, G. (2015). Silk microfiber-reinforced silk hydrogel composites for functional cartilage tissue repair. Acta Biomater. *11*, 27–36.

18. Cho, H., Bucciarelli, A., Kim, W., Jeong, Y., Kim, N., Jung, J., Yoon, S., and Khang, G. (2020). Natural Sources and Applications of Demineralized Bone Matrix in the Field of Bone and Cartilage Tissue Engineering. In Bioinspired Biomaterials. Advances in Experimental Medicine and Biology, H.J. Chun, R. Reis, A. Motta, and G. Khang, eds. (Springer), pp. 3–14.

19. Tirta Nindhia, T.G., Koyoshi, Y., Kaneko, A., Sawada, H., Ohta, M., Hirai, S., and Uo, M. (2008). Hydroxyapatite-silk functionally graded material by pulse electric current sintering. Trends Biomater. Artif. Organs *22*, 25–29.

20. Tao, Y., Xu, W., Yan, Y., and Wu, H. (2012). Structure and properties of composites compression-molded from silk fibroin powder and waterborne polyurethane. Polym. Adv. Technol. *23*, 639–644.

21. Kaneko, A., Tamada, Y., Hirai, S., Kuzuya, T., and Hashimoto, T. (2012). Characterization of a silk-resinified compact fabricated using a pulse-energizing sintering device. Macromol. Mater. Eng. *297*, 272–278.

22. Bucciarelli, A., Chiera, S., Quaranta, A., Yadavalli, V.K., Motta, A., and Maniglio, D. (2019). A Thermal-Reflow-Based Low-Temperature, High-Pressure Sintering of Lyophilized Silk Fibroin for the Fast Fabrication of Biosubstrates. Adv. Funct. Mater. *29*, 1901134.

23. Guo, C., Li, C., Vu, H.V., Hanna, P., Lechtig, A., Qiu, Y., Mu, X., Ling, S., Nazarian, A., Lin, S.J., and Kaplan, D.L. (2020). Thermoplastic moulding of regenerated silk. Nat. Mater. *19*, 102–108.

24. Tuan, H.A., Hirai, S., Tamada, Y., and Akioka, S. (2019). Preparation of silk resins by hot pressing Bombyx mori and Eri silk powders. Mater. Sci. Eng. C *97*, 431–437.

25. Anh Tuan, H., Hirai, S., Inoue, S., Mohammed, A.A.H., Akioka, S., and Ngo Trinh, T. (2020). Fabrication of Silk Resin with High Bending Properties by Hot-Pressing and Subsequent Hot-Rolling. Materials (Basel) *13*, 2716.

26. Liu, K., Shi, Z., Zhang, S., Zhou, Z., Sun, L., Xu, T., Zhang, Y., Zhang, G., Li, X., Chen, L., et al. (2018). A Silk Cranial Fixation System for Neurosurgery. Adv. Healthc. Mater. *7*, e1701359.

27. Luo, K., Yang, Y., and Shao, Z. (2016). Physically Crosslinked Biocompatible Silk-Fibroin-Based Hydrogels with High Mechanical Performance. Adv. Funct. Mater. *26*, 872–880.

28. Kurland, N.E., Dey, T., Kundu, S.C., and Yadavalli, V.K. (2013). Precise patterning of silk microstructures using photolithography. Adv. Mater. *25*, 6207–6212.

29. Kim, S.H., Yeon, Y.K., Lee, J.M., Chao, J.R., Lee, Y.J., Seo, Y.B., Sultan, M.T., Lee, O.J., Lee, J.S., Yoon, S., et al. (2018). Precisely printable and biocompatible silk fibroin bioink for digital light processing 3D printing. Nat. Commun. *9*, 1–14.

30. Bucciarelli, A., Muthukumar, T., Kim, J.S., Kim, W.K., Quaranta, A., Maniglio, D., Khang, G., and Motta, A. (2019). Preparation and Statistical Characterization of Tunable Porous Sponge Scaffolds using UV Cross-linking of Methacrylate-Modified Silk Fibroin. ACS Biomater. Sci. Eng. *5*, 6374–6388.

31. Applegate, M.B., Partlow, B.P., Coburn, J., Marelli, B., Pirie, C., Pineda, R., Kaplan, D.L., and Omenetto, F.G. (2016). Photocrosslinking of Silk Fibroin Using Riboflavin for Ocular Prostheses. Adv. Mater. *28*, 2417–2420.

32. Sun, W., Incitti, T., Migliaresi, C., Quattrone, A., Casarosa, S., and Motta, A. (2016). Genipin-crosslinked gelatin-silk fibroin hydrogels for modulating the behaviour of pluripotent cells. J. Tissue Eng. Regen. Med. *10*, 876–887.

33. Chirila, T.V., Suzuki, S., and Papolla, C. (2017). A comparative investigation of *Bombyx mori* silk fibroin hydrogels generated by chemical and enzymatic cross-linking. Biotechnol. Appl. Biochem. *64*, 771–781.

34. Yang, Y.J., Ganbat, D., Aramwit, P., Bucciarelli, A., Chen, J., Migliaresi, C., and Motta, A. (2019). Processing keratin from camel hair and cashmere with ionic liquids. Express Polym. Lett. *13*, 97–108.

35. Butler, M.F., Ng, Y.F., and Pudney, P.D.A. (2003). Mechanism and kinetics of the crosslinking reaction between biopolymers containing primary amine groups and genipin. J. Polym. Sci. A Polym. Chem. *41*, 3941–3953.

36. Elliott, W.H., Bonani, W., Maniglio, D., Motta, A., Tan, W., and Migliaresi, C. (2015). Silk Hydrogels of Tunable Structure and Viscoelastic Properties Using Different Chronological Orders of Genipin and Physical Cross-Linking. ACS Appl. Mater. Interfaces *7*, 12099–12108.

37. Motta, A., Maniglio, D., Migliaresi, C., Kim, H.J., Wan, X., Hu, X., and Kaplan, D.L. (2009). Silk fibroin processing and thrombogenic responses. J. Biomater. Sci. Polym. Ed. *20*, 1875–1897.

38. Do, S.G., Park, J.H., Nam, H., Kim, J.B., Lee, J.Y., Oh, Y.S., and Suh, J.G. (2012). Silk fibroin hydrolysate exerts an anti-diabetic effect by increasing pancreatic β cell mass in C57BL/KsJ-db/db mice. J. Vet. Sci. *13*, 339–344.

39. Reddy, N., and Yang, Y. (2010). Structure and properties of ultrafine silk fibers produced by Theriodopteryx ephemeraeformis. J. Mater. Sci. *45*, 6617–6622.

40. Montgomery, D.C. (2012). Design and Analysis of Experiments, Eighth Edition (Wiley).

41. Bucciarelli, A., Greco, G., Corridori, I., Pugno, N.M., and Motta, A. (2021). A Design of Experiment Rational Optimization of the Degumming Process and Its Impact on the Silk Fibroin Properties. ACS Biomater. Sci. Eng. *7*, 1374–1393.

42. Bucciarelli, A., Olivetti, E., Adami, A., and Lorenzelli, L. (2021). Design of experiment rational optimization of an inkjet deposition of silver on Kapton. IEEE Sens. J. https://doi.org/10.1109/JSEN.2021.3058543.

43. Bossi, A.M., Bucciarelli, A., and Maniglio, D. (2021). Molecularly Imprinted Silk Fibroin Nanoparticles. ACS Appl. Mater. Interfaces *13*, 31431–31439.

44. Bucciarelli, A., Greco, G., Corridori, I., Motta, A., and Pugno, N.M. (2021). Tidy dataset of the experimental design of the optimization of the alkali degumming process of Bombyx mori silk. Data Brief *38*, 107294.

45. Gaiardo, A., Novel, D., Scattolo, E., Crivellari, M., Picciotto, A., Ficorella, F., Iacob, E., Bucciarelli, A., Petti, L., Lugli, P., and Bagolini, A. (2021). Optimization of a Low-Power Chemoresistive Gas Sensor: Predictive Thermal Modelling and Mechanical Failure Analysis. Sensors (Basel) *21*, 783.

46. Gaiardo, A., Novel, D., Scattolo, E., Bucciarelli, A., Bellutti, P., and Pepponi, G. (2021). Dataset of the Optimization of a Low Power Chemoresistive Gas Sensor: Predictive Thermal Modelling and Mechanical Failure Analysis. Data (Basel) *6*, 30.

47. Rohatgi, C.V., Dutta, N.K., and Choudhury, N.R. (2015). Separator Membrane from Crosslinked Poly(Vinyl Alcohol) and Poly(Methyl Vinyl Ether-alt-Maleic Anhydride). Nanomaterials (Basel) *5*, 398–414.

48. Dimida, S., Barca, A., Cancelli, N., De Benedictis, V., Raucci, M.G., and Demitri, C. (2017). Effects of Genipin Concentration on Cross-Linked Chitosan Scaffolds for Bone Tissue Engineering: Structural Characterization and Evidence of Biocompatibility Features. Int. J. Polym. Sci. *2017*, 1–8.

49. Wang, L., Wang, Y., Qu, J., Hu, Y., You, R., and Li, M. (2013). The Cytocompatibility of Genipin-Crosslinked Silk Fibroin Films. J. Biomater. Nanobiotechnol. *04*, 213–221.

50. Smith, B.C. (2016). Distinguishing Structural Isomers: Mono- and Disubstituted Benzene Rings. Spectroscopy (Springf.) *31*, 36–39.

51. Hasirci, V., Yilgor, P., Endogan, T., Eke, G., and Hasirci, N. (2011). Polymer fundamentals:

polymer synthesis. In Comprehensive Biomaterials, P. Ducheyne, K.E. Healy, D.W. Hutmacher, D.W. Grainger, and C.J. Kirkpatrick, eds. (Elsevier), pp. 349–371.

52. Ninh, C., Iftikhar, A., Cramer, M., and Bettinger, C.J. (2015). Diffusion–reaction models of genipin incorporation into fibrin networks. J. Mater. Chem. B Mater. Biol. Med. *3*, 4607–4615.

53. Marelli, B., Patel, N., Duggan, T., Perotto, G., Shirman, E., Li, C., Kaplan, D.L., and Omenetto, F.G. (2017). Programming function into mechanical forms by directed assembly of silk bulk materials. Proc. Natl. Acad. Sci. USA *114*, 451–456.

54. Motta, A., Fambri, L., and Migliaresi, C. (2002). Regenerated silk fibroin films: thermal and dynamic mechanical analysis. Macromol. Chem. Phys. *203*, 1658–1665.

55. Yuan, Q., Yao, J., Huang, L., Chen, X., and Shao, Z. (2010). Correlation between structural and dynamic mechanical transitions of regenerated silk fibroin. Polymer (Guildf.) *51*, 6278–6283.

56. Wang, J., Guan, J., Hawkins, N., and Vollrath, F. (2018). Analysing the structure and glass transition behaviour of silks for archaeology and conservation. J. R. Soc. Interface *15*, 20170883.

57. Porter, D., Vollrath, F., and Shao, Z. (2005). Predicting the mechanical properties of spider silk as a model nanostructured polymer. Eur Phys J E Soft Matter *16*, 199–206.

58. Flores, R., Perez, J., Cassagnau, P., Michel, A., and Cavaillé, J.Y. (1996). Dynamic mechanical behavior of poly(vinyl chloride)/poly(methyl methacrylate) polymer blend. J. Appl. Polym. Sci. *60*, 1439–1453.

59. Uma Devi, L., Bhagawan, S.S., and Thomas, S. (2010). Dynamic mechanical analysis of pineapple leaf/glass hybrid fiber reinforced polyester composites. Polym. Compos. *31*, 956–965.

60. Chee, S.S., Jawaid, M., Sultan, M.T.H., Alothman, O.Y., and Abdullah, L.C. (2019). Thermomechanical and dynamic mechanical properties of bamboo/woven kenaf mat reinforced epoxy hybrid composites. Compos. Part B Eng. *163*, 165–174.

61. Fessel, G., Cadby, J., Wunderli, S., van Weeren, R., and Snedeker, J.G. (2014). Dose- and time-dependent effects of genipin crosslinking on cell viability and tissue mechanics - toward clinical application for tendon repair. Acta Biomater. *10*, 1897–1906.

62. Zhang, Q., Wang, X., Mu, Q., Liu, P., Jia, S., Chen, L., Zhang, X., Wang, K., and Wei, Y. (2015). Genipin-cross-linked silk sericin/poly(N-isopropylacrylamide) IPN hydrogels: color reaction between silk sericin and genipin, pore shape and thermo-responsibility. Mater. Chem. Phys. *166*, 133–143.

63. Hu, X., Kaplan, D., and Cebe, P. (2006). Determining Beta-Sheet Crystallinity in Fibrous Proteins by Thermal Analysis and Infrared Spectroscopy. Macromolecules *39*, 6161–6170.

64. Ruggeri, F.S., Longo, G., Faggiano, S., Lipiec, E., Pastore, A., and Dietler, G. (2015). Infrared nanospectroscopy characterization of oligomeric and fibrillar aggregates during amyloid formation. Nat. Commun. *6*, 7831.

65. Li, M., Ogiso, M., and Minoura, N. (2003). Enzymatic degradation behavior of porous silk fibroin sheets. Biomaterials *24*, 357–365.

66. Cao, Y., and Wang, B. (2009). Biodegradation of silk biomaterials. Int. J. Mol. Sci. *10*, 1514–1524.

67. R Development Core Team (2019). R: A Language and Environment for Statistical Computing (R Foundation for Statistical Computing).

68. Bucciarelli, A., Reddy Chandraiahgari, C., Adami, A., Mulloni, V., and Lorenzelli, L. (2020). Precise dot inkjet printing thought multifactorial statistical optimization of the piezoelectric actuator waveform. Flex. Print. Electron. *5*, 045002.

69. Bucciarelli, A., Adami, A., Chandaiahgari, C.R., and Lorenzelli, L. (2020). Multivariable optimization of inkjet printing process of Ag nanoparticle ink on Kapton. In 2020 IEEE International Conference on Flexible and Printable Sensors and Systems (FLEPS) (IEEE), pp. 1–4.